Engineering Structures 308 (2024) 118046

Contents lists available at ScienceDirect

Engineering Structures

journal homepage: www.elsevier.com/locate/engstruct

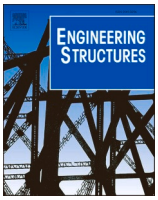

Time-dependent soil–structure interaction analysis using a macro-element foundation model

Bo Liu [a,b], Jianfeng Xue [a,*], Barry M. Lehane [c], Zhen-Yu Yin [b]

[a] School of Engineering & Technology, The University of New South Wales, Canberra 2612, Australia
[b] Department of Civil and Environmental Engineering, The Hong Kong Polytechnic University, Hung Hom, Kowloon 999077, the Hong Kong Special Administrative Region of China
[c] School of Engineering, The University of Western Australia, WA 6009, Australia

ARTICLE INFO

Keywords:
Soil–structure interaction
Creep settlement
Macro-element modelling
Load redistribution
Differential settlement

ABSTRACT

The delayed settlement of foundations due to soil consolidation, creep or particle breakage can alter the internal load distribution and differential settlements in a superstructure through soil–structure interaction (SSI). The study introduces a novel methodology to simulate time-dependent SSI that overcomes the complexity of incorporating the time-dependent behaviour of foundations into routine SSI analysis. The proposed approach represents the superstructure as a condensed stiffness matrix, and replaces the foundations and underlying soils with macro-element foundation models that encapsulate the foundation–soil interaction into load–displacement relationships derived from constitutive models. To examine the performance of the proposed method, a macro-element model for time-dependent analysis of shallow foundations on sand was integrated with structural analysis to simulate two tests performed in a geotechnical centrifuge on a 3D-printed aluminium framed structure supported by footings on sand. The simulated responses of the superstructure and foundations were found to agree well with those observed in the centrifuge tests. Parametric analyses were conducted to investigate the effect of loading history, load level on the superstructure, and creep tendency of soil on post-construction load redistribution and differential settlements. The findings suggest that creep of foundations on sand facilitates load redistribution in the structure from heavily loaded sections to lightly loaded sections. Moreover, post-construction load redistribution depends on the differential creep between footings and should be considered for structures that are quickly constructed or at high levels of strength mobilisation (low factor of safety). Overall, the study highlights the potential of the proposed methodology in analysing the time-dependent SSI and its applicability in practical SSI analysis.

1. Introduction

The interaction between the superstructure and its foundations is often ignored in the conventional design process where the column bases are assumed to be fixed and the load is distributed to columns according to the tributary areas of columns. However, in reality, differential settlements between the columns can lead to a redistribution of loads in the structure, causing stress states of the structure different to those predicted in the conventional design process. Case histories and physical experiments [1–3] show that the load redistributed to or from a foundation due to soil–structure interaction (SSI) under static loading can be up to 40% of its design load. This highlights the need for interactive SSI analysis that considers the superstructure, foundation and underlying soil as a compatible system. Numerous numerical studies in the literature have revealed that the magnitude of the SSI effect is influenced by many factors, including the ratio of the stiffness of the superstructure to that of the substructure [4–6], the sequence of load application during and after construction [7–9] and the design details of the superstructure and foundations [10–16].

There is a significant lack of knowledge regarding the time dependency of SSI in the literature, despite the fact that delayed settlements of foundations due to soil consolidation [17–19], creep [20,21], particle breakage [22–24] or their combinations can contribute greatly to the overall settlement. In early studies [25–27], the importance of

* Corresponding author.
E-mail addresses: bo-robert.liu@polyu.edu.hk (B. Liu), jianfeng.xue@adfa.edu.au (J. Xue), barry.lehane@uwa.edu.au (B.M. Lehane), zhenyu.yin@polyu.edu.hk (Z.-Y. Yin).

https://doi.org/10.1016/j.engstruct.2024.118046
Received 7 June 2023; Received in revised form 5 April 2024; Accepted 10 April 2024
Available online 19 April 2024

time-dependent SSI is evaluated indirectly by comparing the immediate and the long-term/stable states of superstructures, using the undrained and drained moduli of soils for studying the immediate and long-term behaviours, respectively. Implicit in the rationale of these works is an assumption that the most unfavourable loading condition would occur at either the immediate or the long-term state, and the intermediate states could be safely ignored. However, the validity of this assumption was questioned by a later finite element analysis of SSI conducted by Viladkar et al. [28], who showed that the peak values of differential settlements occurred at an intermediate state for a space frame on a viscoelastic soil. Ai et al. [29] developed a semi-analytical and semi-numerical method for time-dependent analysis of superstructures on a cross-anisotropic viscoelastic soil considering the combined effect of creep and consolidation. The study showed that whether the most unfavourable condition occurs at an intermediate state or not depends on the viscosity and anisotropy of the soil. In contrast, Nasri and Magnan [30] found that differential settlements reached a minimum at an intermediate consolidation state in a framed structure supported by a raft. This phenomenon was attributed to the shorter drainage path of soils at the edge of the raft.

Although the studies mentioned above have provided some insights into the characteristics of time-dependent SSI, the soil/foundation models used in these studies – viscoelastic models based on finite element method or analytical solutions – are too complex and require many model parameters, making them unsuitable for practical application. Moreover, almost all existing studies discussed above only involve numerical investigations which are not verified by measured responses of real-life structures or physical models. Therefore, these studies can lead to predictions that are not compatible with field observations. For instance, most of the studies assume the existence of a final stable state, whereas field observations show that the settlement of structures on both sand [21,31,32] and clay [17,19,33] can continue to increase for decades with no tendency to stabilise. Additionally, the emphasis in most studies has been placed on the SSI induced by the consolidation settlement of foundations on clay, while the creep of foundations has received much less attention.

This study focuses on the SSI induced by the creep behaviour of foundations and addresses the aforementioned issues by introducing a novel method for time-dependent SSI analysis. The proposed method utilises the one-dimensional (1D) elasto-viscoplastic macro-element model proposed by the authors [34] to simulate the creep behaviour of shallow foundations. The macro-element approach, initially proposed by Nova and Montrasio [35], directly simulates the load–displacement behaviour of foundations without explicitly considering the foundation soils. In this approach, a foundation is modelled as a single element where a constitutive relationship that encapsulates the foundation–soil interaction is established between the load and settlement of foundations.

Compared to finite element or semi-analytical foundation models used in previous studies, the macro-element model is computationally efficient, yet still able to incorporate the nonlinear, loading history- and time-dependent behaviours of foundations into SSI analysis, provided an appropriate constitutive theory is employed. The 1D elasto-viscoplastic macro-element model proposed by the authors [34] is among the few macro-element models that consider the time-dependent behaviour of foundations and has been shown to be capable of satisfactorily predicting the creep behaviours of shallow foundations on sand under typical working load conditions [36].

In the proposed method, the foundation responses are simulated using the macro-element foundation model, while the superstructure is simplified as a "condensed" structural stiffness matrix. Notably, the macro-element model has only three parameters, two of which are the bearing capacity and elastic footing stiffness which are routinely used in practice. The third parameter quantifies the tendency of a footing to creep and can be determined by in-situ plate load tests. These characteristics allow the method to be easily adopted in practical SSI analysis.

The performance of the proposed method is for the first time examined using centrifuge tests on a 3D-printed model frame supported by isolated footings on sand [2]. Subsequently, parametric analyses are conducted to reveal the effect of factors such as the number of load increments, loading rate, load magnitude and creep tendency of soil on the long-term SSI.

2. A coupled superstructure–foundation simulation method

2.1. Model for superstructure–foundation interaction

In this study, the superstructure is considered as a linear elastic system so that it can be conveniently simulated by a "condensed" structural stiffness matrix [5]. It is noted that the macro-element model can also be incorporated into other types of structural analysis, such as finite element analysis. Besides, the superstructure is subjected to vertical quasi-static loads, and the foundations are assumed to displace vertically only with no lateral/rotational movements. This is appropriate for framed structures designed with the strong column–weak beam principle [37]. Sensitivity analysis conducted using the finite element model of the 3-storey framed structure (to be introduced in Section 3) reveals that considering the lateral and rotational degrees of freedom has a negligible effect of less than 2% on the calculated column forces and foundation settlements. As the time dependency of the system is dominated by that of the soil, the time-dependent behaviour of the superstructure is neglected in this study.

For the analysis of superstructure–foundation interaction, the state of the superstructure can be characterised by two vectors:

1) the vector of displacements at the column bases, denoted as $\boldsymbol{s}$, and
2) the vector of reaction forces at the column bases (or the footing loads), denoted as $\boldsymbol{N}$.

These two vectors are related to each other through [5]:

$$\boldsymbol{N} = \boldsymbol{N}_0 + \boldsymbol{M}^{\mathrm{S}}\boldsymbol{s} \tag{1}$$

where $\boldsymbol{N}_0$ is the reaction force vector of the same superstructure with rigidly supported column bases (conventional design condition); $\boldsymbol{M}^{\mathrm{S}}$ is the condensed structural matrix. The component M^{S}_{ij} of the condensed structure matrix represents the reaction force induced at the base of column i due to a unit displacement at the base of column j. For example, the component M^{S}_{31} indicates the reaction force induced at support 3 (R_3) by a unit displacement at footing 1 while keeping other footings fixed as shown in Fig. 1. The condensed structure matrix can be obtained using the substructure method [38,39] or by performing simulations where a unit displacement is applied to each column in turn, as shown in

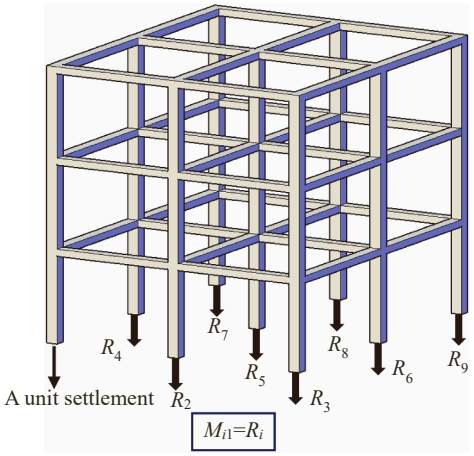

Fig. 1. Physical significance of condensed structure matrix.

Fig. 1.

In the general cases where each column base has six degrees of freedom, the size of the condensed matrix is $6n \times 6n$ where n is the number of columns. Because the lateral/rotational displacements of foundations are neglected in this study, the superstructure can be modelled as an $n \times n$ condensed matrix. In this case, the force equilibrium of the superstructure can be written as:

$$\sum_{i=1}^{n} M_{ij}^{S} = 0 \tag{2}$$

Eq. (2) is used to obtain the diagonal components M_{ii}^{S}.

Besides, if the superstructure settles uniformly with no differential settlement, there will be no load redistribution among the superstructure, i.e. $\boldsymbol{N}$=$\boldsymbol{N}_0$. This dictates the following property of the condensed structure matrix:

$$\sum_{j=1}^{n} M_{ij}^{S} = 0$$

For the purpose of the SSI analysis, the foundation equation can be expressed as:

$$\boldsymbol{s} = \boldsymbol{M}^{F}\boldsymbol{N} \tag{3}$$

where $\boldsymbol{M}^{F}$ is the foundation flexibility matrix relating the vector of support reactions ($\boldsymbol{N}$) to the vector of support displacements ($\boldsymbol{s}$). The size of the foundation flexibility matrix is the same as the condensed structure matrix. In cases such as the piled raft foundation considered by Leung et al. [12], the off-diagonal components of $\boldsymbol{M}^{F}$ are non-zero, meaning that the displacement at one support may be affected by the reaction forces at other supports.

For isolated footings with negligible interactions between each other, which is the case considered in this study, the foundation flexibility matrix is a diagonal matrix with all off-diagonal components being zero. Besides, when the nonlinear, loading history- and time-dependent behaviour of footings is concerned, $\boldsymbol{M}^{F}$ will change with $\boldsymbol{N}$, time and loading history.

Combining Eqs. (1) and (3), an equation governing the performance of the superstructure–foundation system is obtained [4,8]:

$$\left(\boldsymbol{E} - \boldsymbol{M}^{S}\boldsymbol{M}^{F}\right)\boldsymbol{N} = \boldsymbol{N}_0 \tag{4}$$

where $\boldsymbol{E}$ is an identity matrix of the same order as $\boldsymbol{M}^{S}$.

2.2. The 1D elasto-viscoplastic macro-element foundation model

In this study, during the solution process of Eq. (4), the foundation flexibility matrix $\boldsymbol{M}^{F}$ was obtained and updated using the 1D elasto-viscoplastic macro-element model proposed by the authors [34]. The model can capture several time effects seen in practice, such as the settlement increase during slow unloading, the post-creep stiffening effect and the settlement induced by unload–reload cycles. The model's performance has been validated with a foundation database comprising more than 50 footing load tests on sand [36].

In this macro-element model, a time-dependent constitutive relationship is established between the normalised bearing stress $q_n = q/q_f$ (macro-stress) and the normalised foundation settlement $S_n = s/B$ (macro-strain) where q is the bearing stress, q_f the bearing capacity defined as the bearing stress at $S_n = 0.1$, s the foundation settlement and B the foundation width. The macro-element model is formulated based on the non-stationary flow surface theory [40,41], where the total macro-strain increment (dS_n) is decomposed using Eq. (5) into an elastic part (dS_n^e) and a viscoplastic part (dS_n^{vp}).

$$dS_n = dS_n^e + dS_n^{vp} \tag{5}$$

The elastic strain increment is related to the increment of the macro-stress increment (dq_n) through Eq. (6).

$$dS_n^e = \frac{dq_n}{K} \tag{6}$$

where K is the non-dimensional elastic stiffness of footing which can be calculated as $K = k_i/q_f$ in which k_i can be determined with the small-strain shear modulus (G_0) of soil using [42]:

$$k_i = \frac{8G_0}{\pi(1-\nu)} \tag{7}$$

where Poisson's ratio ν can be taken as 0.1 when only the elastic range of soil response is concerned [43,44]. Eq. (7), originally derived for circular foundations, can be extended to rectangular foundations by utilizing shape factors derived from existing studies on the settlement of shallow foundations on elastic half-space, such as Gazetas et al. [45], Brothers et al. [46], and Baraldi and Tullini [47]. However, since the shape factor for square foundations derived from Gazetas et al. [45] is 0.86 and elastic settlement constitutes only a small portion of the total settlement, Eq. (7) is directly applied to square foundations in this study.

The magnitude of viscoplastic strain increment (dS_n^{vp}) is regulated by the consistency requirement that any viscoplastic state must lie on the flow surface f, which dictates $df = 0$. The flow function f is formulated based on field observations of footing responses as follows:

$$f = \frac{q_n^2}{K(1-q_n)} + cq_n^2 \ln\left(\frac{\dot{S}_n^{vp,ref}}{\dot{S}_n^{vp}}\right) - S_n^{vp} \tag{8}$$

where $\dot{S}_n^{vp,ref}$ is a reference strain rate which is assumed to be high enough to eliminate the occurrence of creep, set to 0.01 s^{-1} as a default; $\dot{S}_n^{vp}$ is the viscoplastic strain rate to be determined and c is a model parameter which measures the creep tendency of soils. The creep parameter can be related to the rate of creep settlement development through [48]:

$$\frac{s_c}{B} = c\left(\frac{q}{q_f}\right)^2 \ln\left(\frac{t}{t_{ref}}\right) \tag{9}$$

where s_c is the creep settlement, t_{ref} is a reference time, and t is the creep time.

In this study, the increment of the reaction force vector ($d\boldsymbol{N}$) corresponds to the increments of macro-stresses on footings. For each footing, the elastic increment of the macro-strain associated with the macro-stress increment can be calculated from Eq. (6) whereas the viscoplastic increment is determined by solving $df = 0$ with f defined in Eq. (8). In this study, $df = 0$ is solved using the Newton-Raphson method to determine $\dot{S}_n^{vp}$, and dS_n^{vp} is calculated as $\dot{S}_n^{vp} \bullet dt$ where dt is the timestep. The Newton-Raphson method is used due to its simplicity, rapid convergency and robustness in solving a diverse range of nonlinear equations. Three parameters are involved in simulating the behaviour of footings on sand using the macro-element model: the elastic stiffness k_i, the bearing capacity q_f and the creep parameter c. The first two parameters are routinely used in practice and can be estimated with good accuracy from a seismic cone penetration test conducted adjacent to the footing [49,50]. The creep parameter was originally proposed by Lehane et al. [48] based on the settlement observations of several field footings on sand. According to Eq. (9), this parameter quantifies the stress-level dependency of the slope of $s_c/B - \ln(t)$ curve. Therefore, c can be determined from plate load tests with several creep stages at different stress levels [34]. Liu [36] showed that the typical values of c range from 0.002 to 0.02 for siliceous sands and could be 0.03 or higher for calcareous sands. More details of the macro-element model can be found in [34].

2.3. Implementation procedures

In the numerical scheme, the loading process of the superstructure is divided into many small steps. At each of these steps, Eq. (4) is solved using the Gauss-Seidel method to obtain the reaction force vector ($\boldsymbol{N}$) and the settlement vector ($\boldsymbol{s}$). The foundation flexibility matrix ($\boldsymbol{M}^{S}$) is updated using the macro-element model during the iterations. The algorithm used in a timestep to obtain the reaction force vector $\boldsymbol{N}$ and the settlement vector $\boldsymbol{s}$ for a prescribed increment of loads on the superstructure is illustrated in Fig. 2. In this figure, UDL is the uniformly distributed load and N_d is the dead load. Note that even when the load on the superstructure remains constant (dUDL and dN_d are zero), the reaction force and settlement will vary over time. This is attributed to the use of the elasto-viscoplastic model for simulating the foundations. The program was written in FISH language in FLAC^{3D}.

3. Validation of the proposed method

This section examines the implementation and performance of the proposed method using two of the centrifuge tests (tests T3 and T4) conducted by the authors [2]. In the experiments, 3D-printed aluminium frames with isolated spread footings were placed on the surface of soil samples. The centrifuge models were tested under 100 g where g is Earth's gravity. A flexible water tank was placed on top of the structure to apply a UDL by pumping water into the tank during centrifuge spinning. The water tank was constructed using steel mesh with 6×6 mm^2 openings, fabricated with 0.8 mm diameter steel wires. The model structure used in tests T3 and T4 was a 3-storey, 4 bay $\times$ 2 bay

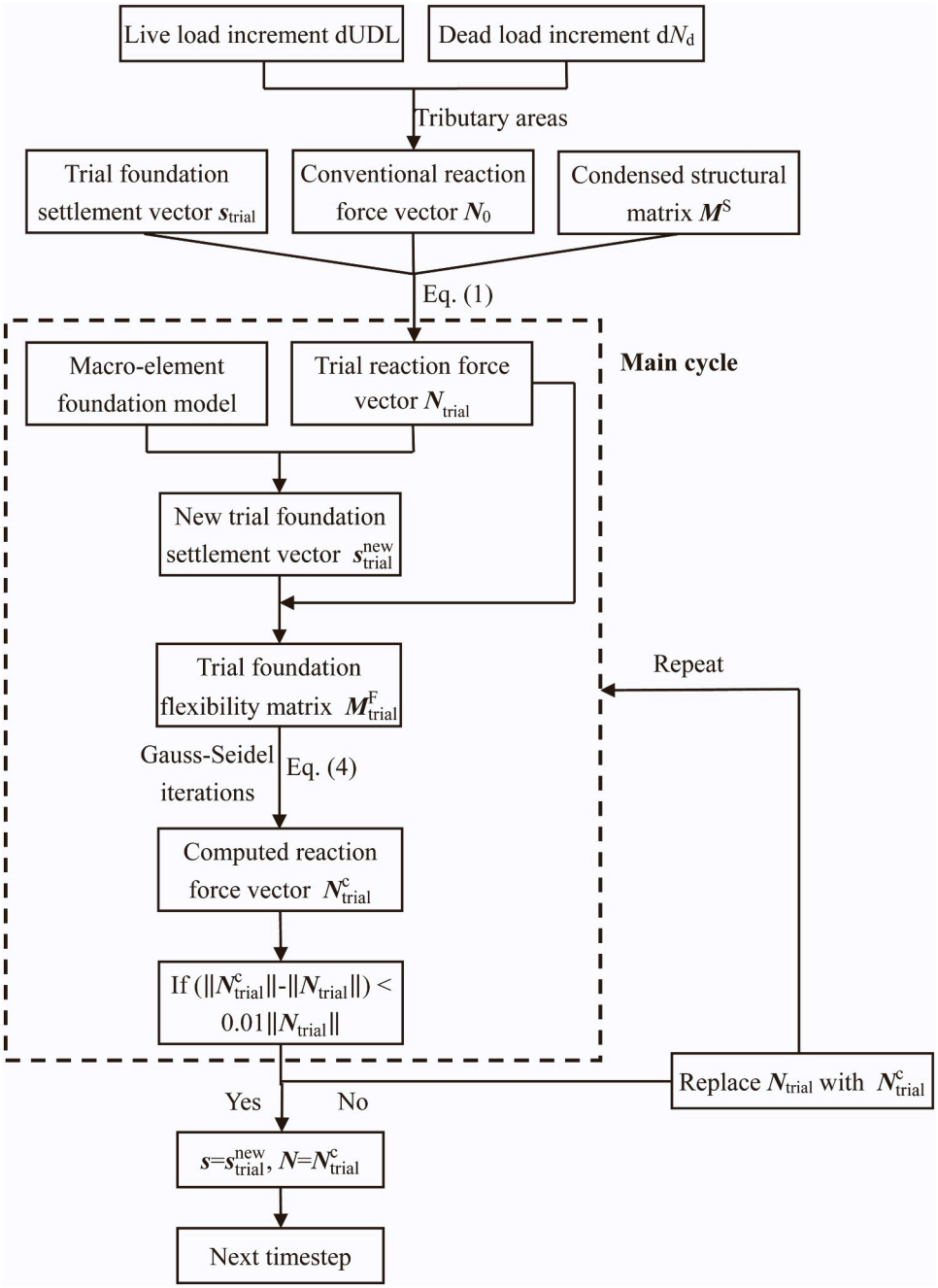

Fig. 2. Algorithm used in a timestep to obtain the reaction force vector and settlement vector (the trial foundation settlement vector above the main cycle takes the value of the settlement vector obtained at the last timestep).

frame, as shown in Fig. 3(a). The dimensions of the structure are indicated on the plan view in Fig. 3(b). The columns were made of 5 mm × 5 mm square hollow sections with 1 mm wall thickness and the beams were solid sections with the width and height of 5 mm and 3 mm respectively. Each storey of the structure was 3D-printed separately, enabling them to be bolted together to form a three-storey structure. The bolted connections were designed at the mid-height of the columns where the bending moment is expected to be small. The properties of the 3D-printed aluminium material are listed in Table 1.

For this structure, the vector $\boldsymbol{N}_0$ representing the load distribution at the conventional design state can be obtained from the tributary areas of the columns, i.e. $N_{0i}=\frac{1}{4}l_1l_2p+N_d$, $\frac{1}{2}l_1l_2p+N_d$ and $l_1l_2p+N_d$ for the corner, side and centre columns, respectively. In the equations, $l_1 = 0.06$ m and $l_2 = 0.07$ m are the bay lengths in the length and width directions respectively; p is the UDL acting on the top floor; N_d is the dead load due to the self-weights of the superstructure and other accessories, which is assumed to be constant in all columns as observed in the experiments.

The condensed structure matrix ($\boldsymbol{M}_s$) was obtained using structural simulations performed in FLAC^{3D}. The numerical model for the 3-storey framed structure was constructed using a collection of linear elastic 'Beam' elements, which is a two-node line-type finite element with 6 degrees of freedom at each node. The numerical model has the same 5 × 3 column scheme as the model structure (5 columns in the longitudinal direction spaced by 60 mm and 3 columns in the transversal direction spaced by 70 mm). The cross-section properties of the beams and columns are calculated according to the corresponding dimensions of the aluminium frame, and Young's modulus and Poisson's ratio of the aluminium are listed in Table 1. The structure elements and their connections are assumed to exhibit linear elastic behaviour with no failure point. The validity of this assumption has been confirmed through simulations of the centrifuge tests using the linear elastic model, which revealed that the maximum stress in the structural members remains below half of the yield strength [2].

Table 1
Properties of the 3D-printed aluminium.

Property	Value (s)
Young's modulus (GPa)	62
Poisson's ratio	0.33
Density (g/cm^3)	2.68
Yield strength (MPa)	250

Note: The yield strength corresponds to an axial tensile strain of 0.2%.

In each simulation, all except one column base were rigidly fixed in all six directions, and the free column was forced to settle vertically by a small displacement. The induced vertical forces in the rigidly fixed columns were used to obtain the components of the condensed structure matrix, as demonstrated in Fig. 1. The structural simulations were conducted in the static, small-strain solution mode in FLAC^{3D}. Typically, time-dependent structural analysis generally requires a fully dynamic mode with the allowance of geometric nonlinearity and energy dissipation through critical damping (e.g. [51–54]). However, in this study, these effects can be disregarded due to the small magnitude of deformations involved in the simulations (because the strength mobilisation level is low, as discussed earlier) and the slow deformation rates associated with soil creep, which do not induce any dynamic effects.

3.1. Validation of the proposed method with the structure model on linear elastic foundations

The proposed method is firstly validated by comparing the simulation results of the proposed method with those simulated with FLAC^{3D}, in which linear elastic foundation models with the same stiffness of k were considered in both methods.

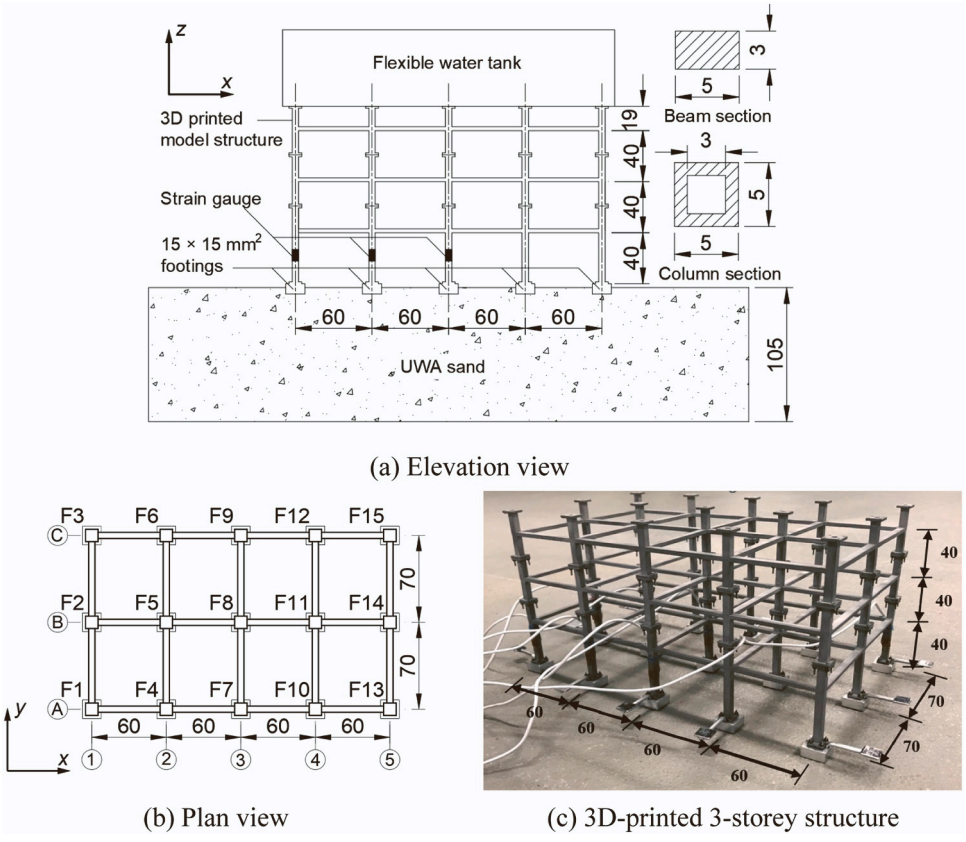

Fig. 3. Details of the 3D-printed aluminium model frame and test set-up; dimensions in mm.

The foundation flexibility matrix ($\boldsymbol{M}^{\mathrm{F}}$) becomes $\frac{1}{k}\boldsymbol{E}$ when the footings have the same stiffness value of k. In this scenario, Eq. (4) is simplified as:

$$\left(\boldsymbol{E}-\frac{1}{k}\boldsymbol{M}^{\mathrm{S}}\right)\boldsymbol{N}=\boldsymbol{N}_0 \tag{10}$$

Eq. (10) is easier to solve numerically compared to Eq. (4) since it does not require determining the foundation flexibility matrix ($\boldsymbol{M}_{\mathrm{F}}$) during iterations using the macro-element model. Therefore, Eq. (10) can be solved directly using the Gauss-Seidel method at any value of $\boldsymbol{N}_0$ without an incremental procedure. However, for validation purposes, the same solution procedure used for solving Eq. (4) was employed to solve Eq. (10).

Fig. 4 compares reaction forces obtained from Eq. (10) and the FLAC^{3D} model for the 3-storey framed structure under a UDL of 30 kPa and $N_{\mathrm{d}}=0$ with different foundation stiffnesses. The corresponding coefficient of variation (CoV) of the reaction forces is also shown in the figure. The CoV of the reaction forces defined in Eq. (11) demonstrates the variation of the forces between the footings.

$$CoV = \frac{s_Q}{\overline{Q}} \tag{11}$$

where $\overline{Q}$ is the mean value of all measured reaction forces Q_i (excluding the dead load N_{d}) and s_Q is the standard deviation of the distribution of all the measured Q_i:

$$s_Q=\left[\sum_{i=1}^{N}(Q_i-\overline{Q})\Big/N\right]^{0.5}$$

Fig. 4(a) shows that the reaction forces on gridlines A and B obtained from the FLAC^{3D} simulation with $k=1\times10^5$ N/m are almost identical to those of the solution of Eq. (10). Besides, both methods predict almost the same CoV of the reaction forces for the foundation stiffness values spanning from 1×10^3 N/m to 1×10^8 N/m, as shown in Fig. 4(b), confirming the reliability of the proposed method.

3.2. Validation of the proposed method with centrifuge tests

The centrifuge tests T3 and T4 were simulated using the proposed method. In these two tests, the 3-storey framed structure was supported by 15×15 mm^2 pad footings founded on dense and medium dense UWA (The University of Western Australia) sand with relative densities of 78% and 58% respectively. The sand is a siliceous sand consisting of sub-rounded to sub-angular grains with a mean particle size of 0.18 mm. The minimum and maximum void ratios of the sand are 0.49 and 0.78, respectively. After the centrifugal acceleration had reached 100 g, the structure was allowed to stabilise for ~1000 s before applying the load through pumping water into the water tank placed on top of the structure. In the centrifuge tests, the water level in the flexible tank was raised in ~10 mm increments (corresponding to a UDL increment of 10 kPa under 100 g), with a 16-min creep period between two successive increments. Under UDL = 10 kPa, the average distributed load on each floor is about 3.3 kPa, which is close to the typical floor loading for residential buildings. The duration of the creep period was selected to allow for a significant portion of creep to occur. The settlements of all footings and the axial forces in a quarter of the columns on the ground floor (F1, F2, F4, F5, F7 and F8; see Fig. 3(b) for locations of the columns) were monitored during the tests. More details of the tests are provided in [2].

In the proposed method, the responses of the footings were simulated using the macro-element model. To model the footings, the bearing capacities (q_{f}) were determined as the bearing stresses observed at $s/B=0.1$ in isolated footing tests conducted adjacent to the framed structure in the centrifuge strongbox. The macro-element has been previously used by the authors [34] to simulate footings on UWA sand. The elastic stiffness (k_{i}) was determined using Eq. (7) with G_0 estimated from the empirical relationship with void ratio developed for UWA sand by Bagbag et al. [55]. The creep parameter (c) was calibrated using the proposed macro-element foundation model to replicate the centrifuge footing tests on UWA sand reported by Liu and Lehane [50]. The macro-element parameters determined accordingly are summarised in Table 2.

In the centrifuge tests, the dead load (N_{d}) increases during the centrifuge ramp-up from normal gravity to the designated acceleration level of 100 g. In this process, the stresses in soils and the bearing capacities of the footings increase. To simulate the footing behaviour using the macro-element model, the bearing capacity was taken as constant throughout the simulation for simplicity. In each centrifuge test, it has been observed that the dead load of the structure has been nearly evenly distributed to the footings. Therefore, the average measured dead load in the corresponding centrifuge test was used as the dead load (N_{d}) on the footings in the macro-element simulations, as listed in Table 2. Note that the value of N_{d} is higher in test T4 because of the additional reinforcement of stiffer steel mesh incorporated on the water tank walls. This reinforcement was implemented to restrict the lateral bulging of the tank after water was added.

In the numerical simulations, the dead load (N_{d}) was applied at a

Table 2
Parameters used to simulate the footings in tests T3 and T4.

Test	k_{i} (MPa)	q_{f} (kPa)	c	N_{d} (N)
T3	83	2115	0.02	25
T4	72	1175	0.02	32

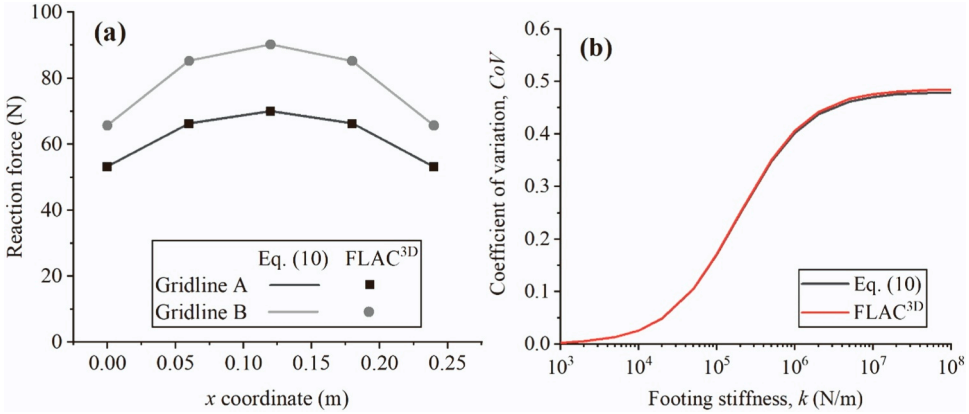

Fig. 4. Comparison between the solution of Eq. (10) and the results of numerical simulation using the FLAC^{3D} model.

constant rate to the footings in 100 s to simulate the ramp-up period of about 100 s and then maintained for another 1000 s to simulate the stabilisation period in the centrifuge tests. After that, the UDL was applied to the superstructure according to the estimated water level history of the centrifuge experiments (see more details in [2]). The histories of UDLs used in the simulations of tests T3 and T4 are presented in Fig. 5.

Figs. 6 and 7 compare the coefficients of variation of the load distribution and the maximum-to-minimum load ratio (Q_{max}/Q_{min}, where Q_{max} and Q_{min} are the maximum and minimum footing loads excluding N_d, respectively) of T3 and T4 obtained from the numerical and experimental simulations. When the UDLs are below about 5 kPa (about 5 mm water in the water tank), the variations of *CoV* and Q_{max}/Q_{min} obtained from the experiments are irregular because the water did not distribute uniformly in the flexible water tank but flocked at lower locations due to the unevenness of the water tank bottom.

For test T3, the values of *CoV* and Q_{max}/Q_{min} predicted in the numerical simulation are greater than those obtained from the centrifuge tests. This is because the lateral bulging of the water tank during the test resulted in more loads being distributed to external columns than predicted from their tributary areas. Consequently, this more evenly distributed load leads to reduced *CoV* and Q_{max}/Q_{min} in the experiment. In test T4 the water tank walls were reinforced to restrain the bulge deformation. Consequently, the *CoV* and Q_{max}/Q_{min} predicted with the proposed method compare favourably with the experimental results at UDL $>$ 5 kPa for this test.

Figs. 6(b) and 7(b) show that the values of *CoV* and Q_{max}/Q_{min} decrease during the creep stages in test T4 and increase initially when the UDL resumes after creep. As loading increases further, the values of these two load distribution factors (*CoV* and Q_{max}/Q_{min}) decrease again. These phenomena are better visualized in Fig. 8 which presents the variation of *CoV* and Q_{max}/Q_{min} with time for test T4. The initial increase and later decrease of *CoV* and Q_{max}/Q_{min} are related to the post-creep behaviour of footings, i.e., the behaviour of the footing during the loading stage following creep. During the creep stages, the centre footings were under higher loads and therefore developed more creep settlements than the corner and side footings, leading to a higher post-creep stiffening effect, i.e. the stiffness of the footing increases after creep. When the UDL application resumes after a creep stage, the values of *CoV* and Q_{max}/Q_{min} first increase because a higher proportion of loads will be distributed to the centre footings whose post-creep stiffening effect is more significant, leading to more non-uniform load distribution. Because the post-creep stiffening effect diminishes as the foundation settlement increases (the phenomenon can be observed in reported field and laboratory footing load tests, e.g. [48,56]), the proportion of loads distributed to centre footings will reduce as load application proceeds, leading to the decrease of *CoV* and Q_{max}/Q_{min} that follows. Fig. 8 also demonstrates that the proposed method is capable of capturing these features. While this behaviour is less significant in later simulations where more realistic loading histories are considered (e.g. Fig. 10), the favourable match between the simulated and experimental results highlights the model's effectiveness in realistically simulating time-dependent SSI.

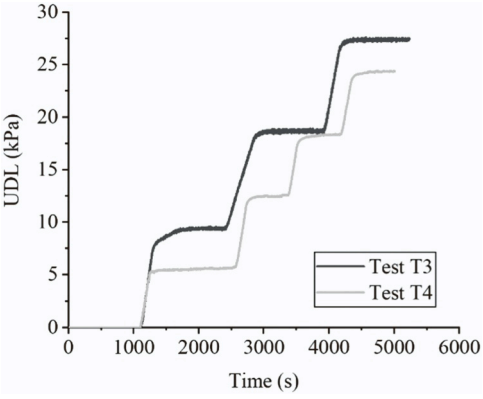

Fig. 5. Variations of UDLs estimated from tests T3 and T4.

4. Parametric analyses

A recent study by Liu [36] has demonstrated that the rate at which load is applied on a footing has a significant influence on the subsequent development of creep settlement. Specifically, a faster loading rate results in less time for creep during the loading stage and correspondingly more after-loading creep settlement. In the centrifuge experiments, the durations allowed for footings to creep were quite short (~1000 s) and the rates of load application were much faster than those in practice. Therefore, it is inferred that the time effects observed in the centrifuge tests are not directly representative of those in real-life structures. To understand the effect of time-dependent foundation behaviour on SSI in more realistic settings, long-term SSI analyses were conducted using the proposed method.

The following parameters were considered in the parametric analyses: the loading history, the duration of the construction/load application, the creep behaviour of the soil and the mobilised strength ratio. In these simulations, the same superstructure and foundations used in centrifuge test T4 were considered because the average footing settlement at the end of the second loading stage (UDL≈12.5 kPa) in this test was about 0.16 mm (16 mm at prototype scale), corresponding to about 1% foundation width; this is a typical foundation settlement at the serviceability limit state.

The load history used in the simulations is illustrated in Fig. 9. For simplicity, the self-weight (dead load), N_d, is not considered in the parametric analyses. The UDL was applied in equal increments to the designated value in a period of T_0. The period T_0 to apply the UDL represents the duration from the start of construction to the full operation of the building. The number of UDL increments is denoted as NS. For simplicity, the duration for each UDL increment was set equal to the duration of the creep pauses between the UDL increments, as shown in Fig. 9. T_0 varies from 1 week to 5 years in the parametric analysis. After the UDL is applied, the building load is maintained for another 50 years.

Omitting the dead load, the total load on the structure can be calculated as G_{total}=UDL·A where $A = 24 \times 14$ m^2 is the area occupied by the building at prototype scale. The overall mobilised strength ratio (R_{mob}) of the considered structure with 15 footings can be defined as:

$$R_{mob} = \frac{G_{total}}{15 q_f B^2}$$

In the numerical simulations, the value of R_{mob} was varied from 0.05 to 0.4 to study the effect of load level on time-dependent SSI. The selected range of R_{mob} corresponds to UDL values ranging from 5.9 to 47.2 kPa.

In addition to the loading conditions, the effect of the creep of the sand on SSI was also studied. The macro-element model parameter c, which characterises the creeping tendency of sand, was varied within the typical range from 0.002 to 0.05, as discussed earlier.

A total of 16 simulations were conducted. The simulation parameters used in the parametric analyses are summarised in Table 3. Note that the default R_{mob}= 0.25 is close to the level of strength mobilisation of the 3-storey framed structure in the centrifuge test T4 at UDL= 12.5 kPa.

In the following analyses, four load distribution indicators are employed to study the SSI. They are the maximum-to-minimum load ratio (Q_{max}/Q_{min}), the coefficient of variation of the load distribution (*CoV*), the differential settlement between footings F7 and F1, denoted as s_7-s_1, and the differential settlement between footings F8 and F7, denoted as s_8-s_7. For the linear elastic superstructure considered in this study, the two differential settlements are proportionally related to the magnitude of load redistribution among the superstructure.

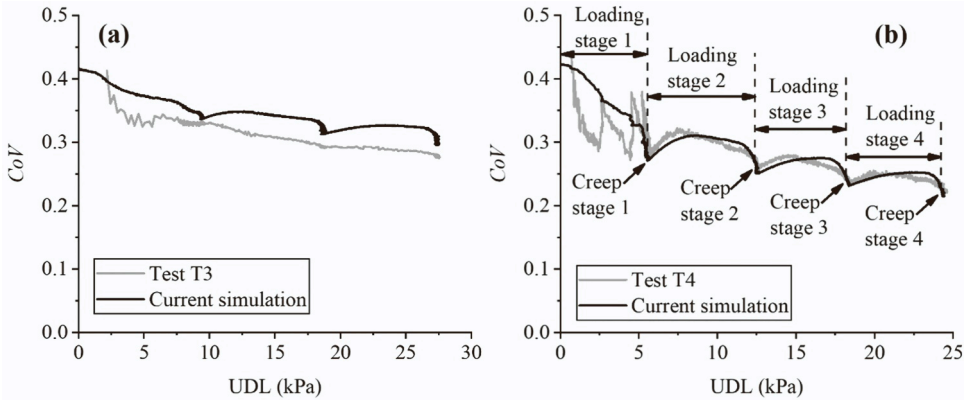

Fig. 6. Comparison of the experimentally and numerically obtained coefficients of variation obtained for (a) test T3 and (b) test T4.

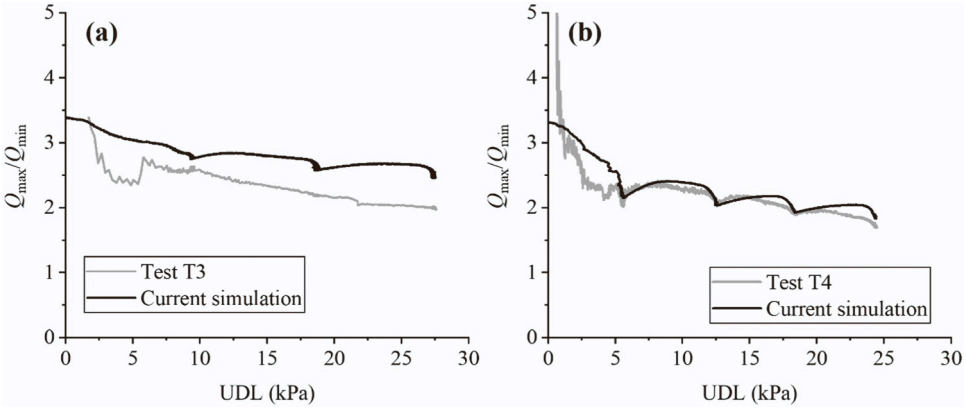

Fig. 7. Comparison of the experimentally and numerically obtained maximum-to-minimum load ratios for (a) test T3 and (b) test T4.

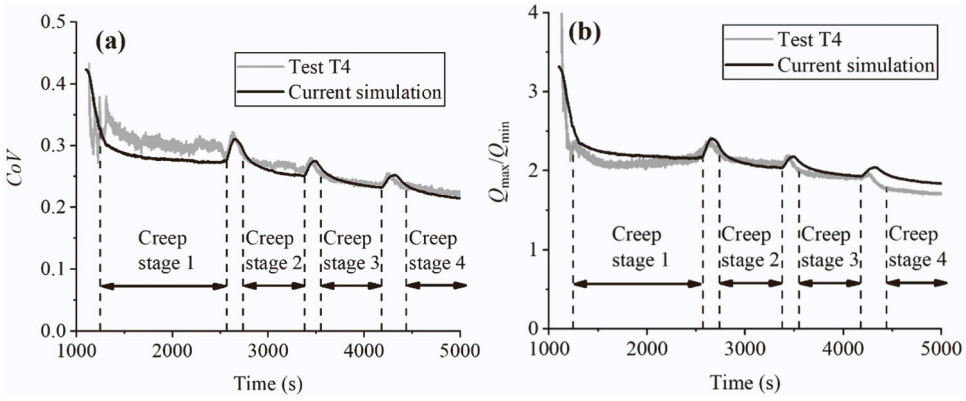

Fig. 8. Variation of (a) the coefficient of variation and (b) maximum-to-minimum ratio of the load distribution with time in test T4.

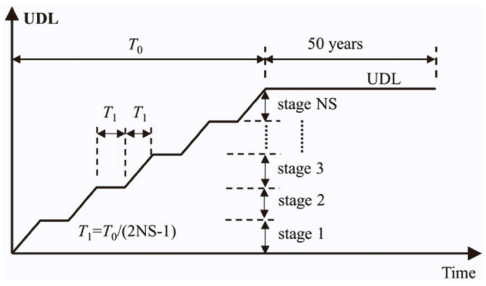

Fig. 9. The load histories used in the simulations.

4.1. Effect of the number of UDL increments (NS)

Fig. 10 presents the variation of the load redistribution indicators with time for the simulations with the same parameters except for NS which varies from 1 to 4. Overall, it is observed from Fig. 10 that although some differences exist within the duration of UDL application (T_0 =1 year), the load distributions among the superstructure at $t > T_0$ are almost identical for the simulations with different NS. This is the basis for using NS= 1 as the default.

Besides, in Figs. 10(a) and 10(b), both the *CoV* and Q_{max}/Q_{min} decreased during the creep stages, indicating that the load redistribution became more uniform. This behaviour is consistent with the centrifuge

Table 3
Summary of the simulation parameters used in the parametric analyses.

Simulation group	Simulation parameters or conditions					
	k_i (MPa)	q_f (kPa)	NS	c	T_0 (year)	R_{mob}
Default	72	1175	1	0.02	1	0.25
Effect of NS	72	1175	2 4	0.02	1	0.25
Effect of creep parameter c	72	1175	1	0.002 0.005 0.01 0.05	1	0.25
Effect of T_0	72	1175	1	0.02	0.019 (1 week) 0.083 (1 month) 0.5 5	0.25
Effect of R_{mob}	72	1175	1	0.02	1	0.05 0.1 0.2 0.3 0.4

test results presented in Fig. 8 and suggests that the creep of footings facilitates load transfer from the centre footings to the corner and side footings. This phenomenon occurs because the creep rate of footing increases with the level of strength mobilisation, as indicated by Eq. (9).

In Fig. 10, it is observed that the differential settlements increase and the load distribution factors (Q_{max}/Q_{min} and CoV) decrease during the 50-year creep period. The associated load transfers are shown in Fig. 11. It is observed that between $t = T_0$ and $t = T_0 + 50$ years, the loads on the corner footings (F1 and F11) increased and those on centre footings (F5, F8 and F11) reduced. Besides, Fig. 10 also suggests that most of the load redistribution and differential settlements occurred during the application of UDL and the post-construction load redistribution is insignificant. This is because the redistribution of loads between footings is controlled by the differential creep rather than the absolute magnitudes of creep settlements. In addition, in the considered structure, loads transfer from the heavily loaded centre footings to the comparatively lightly loaded corner footings. Therefore, as the load redistribution occurs, the difference between the loads on the centre and corner footings reduces, which will in return reduce the rate of differential creep.

4.2. Effect of creep parameter c

Fig. 12 presents the variation of the load distribution factors and differential settlements with time for the simulations with c ranging from 0.002 to 0.05 while keeping the other parameters constant. It is observed from the figure that a more uniform load distribution is obtained when a greater value of c is used, suggesting that more load

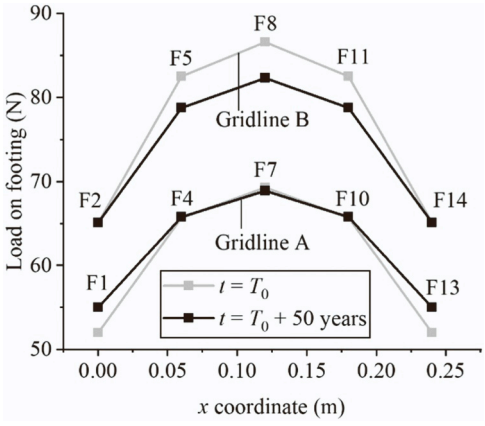

Fig. 11. The distribution of footing loads along gridlines A and B at $t = T_0$ and $t = T_0 + 50$ years.

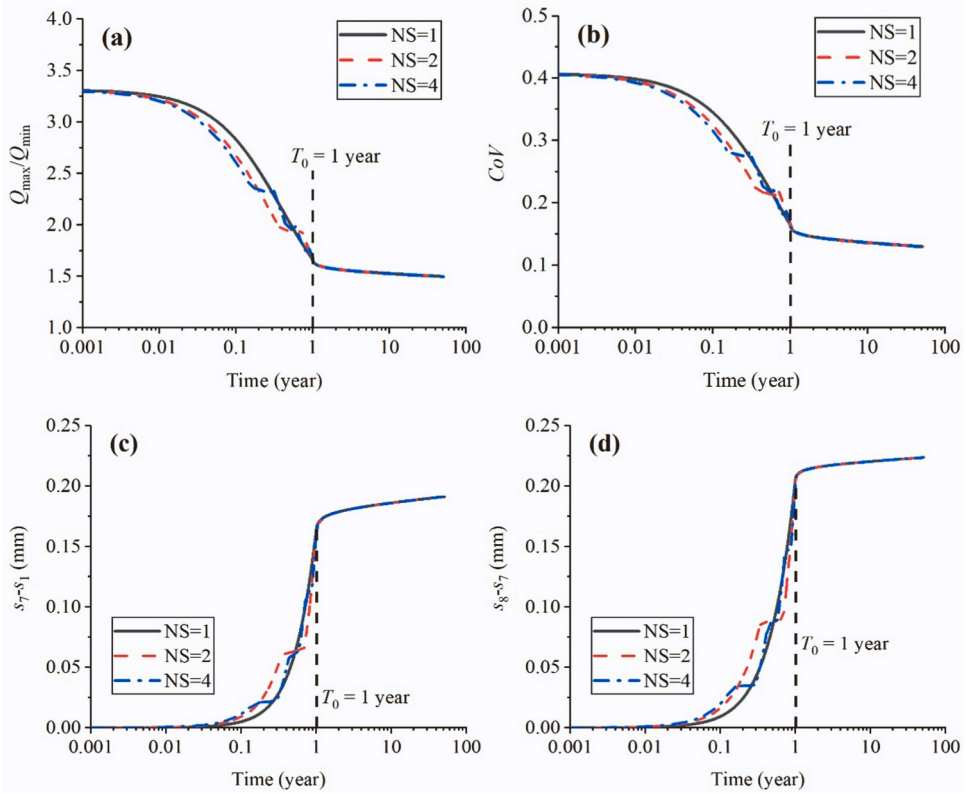

Fig. 10. Effect of the number of loading stages on the load distribution factors and differential settlements: (a) Q_{max}/Q_{min}, (b) CoV, (c) s_7-s_1 and (d) s_8-s_7.

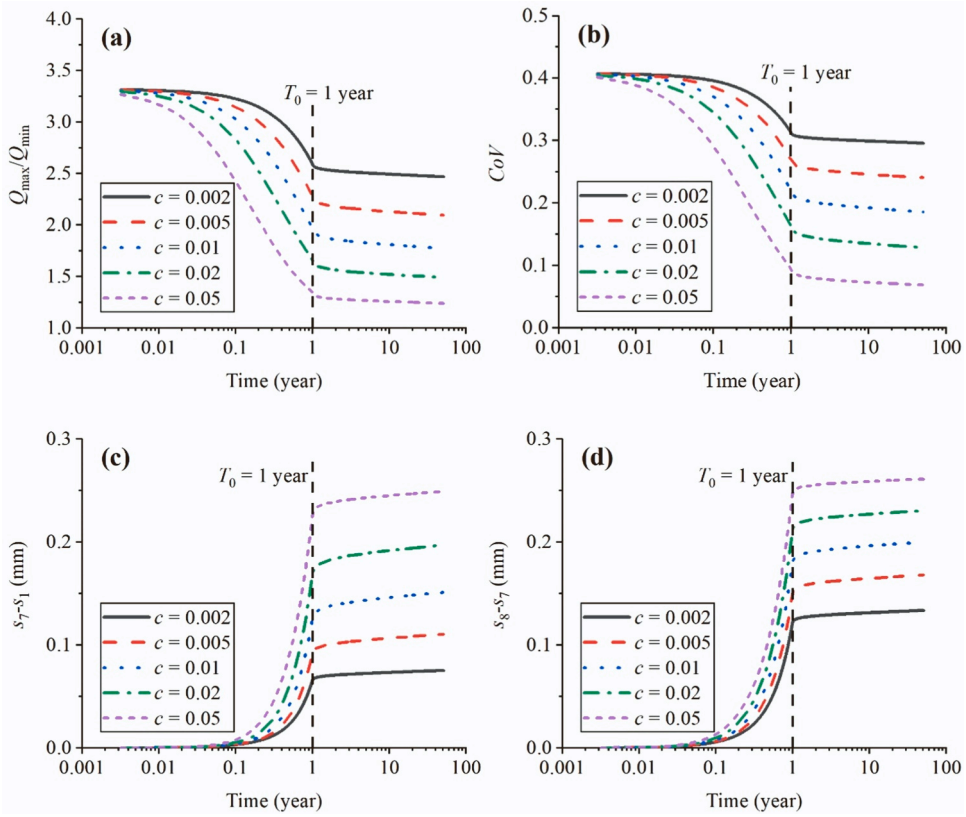

Fig. 12. Effect of creep parameter c on the load distribution factors and differential settlements: (a) Q_{max}/Q_{min}, (b) CoV, (c) s_7-s_1 and (d) s_8-s_7.

redistribution is induced when the foundation soils are more prone to creep. At $t = T_0$, the values of Q_{max}/Q_{min} for $c = 0.002$ and $c = 0.05$ are 2.59 and 1.35, respectively. This indicates that the maximum footing loads (Q_{max}) can differ by 2 times for two identical structures on sands with very different creep tendencies. This highlights the need to evaluate the creep tendency of sands in the design of structures.

Fig. 13(a) presents the increases of differential settlements during the creep period of 50 years between footings F7 and F1, denoted as $\Delta(s_7\text{-}s_1)$, and between footing F8 and F7, denoted as $\Delta(s_8\text{-}s_7)$. For the linear elastic structure considered in the simulations, these two values reflect the magnitude of the load redistribution resulting from 50-year creep. In Fig. 13(a), the differential settlements developed during the creep period increase with c for c values smaller than 0.01. For c greater than 0.02, the post-construction load redistribution reduces with the increase of c.

The load redistribution during the creep period depends on differential creep between the footings which is affected by two factors. One is the creep tendency of sand as it controls the significance of creep effects. The other is the uniformity of load distribution because a more uniform load distribution will generate less differential creep. With the increase of c, the creep tendency of sand increases but the load distribution at $t = T_0$ becomes more uniform (Figs. 12a and 12b). Therefore, when the effect of the uniformity of load distribution at $t = T_0$ overweights that of the creep tendency of sand, load redistribution during the creep period will reduce with the increase of c.

The relative significance of post-construction load redistribution is

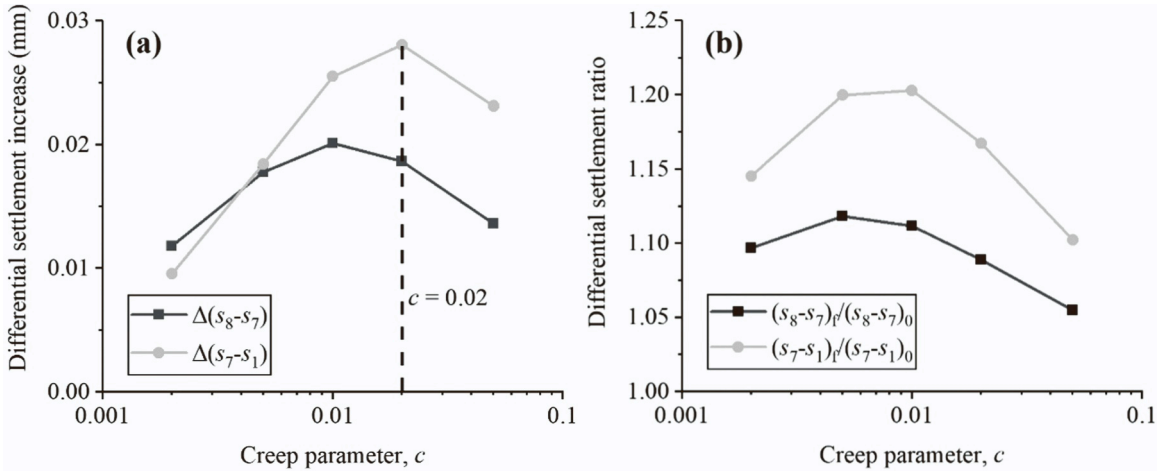

Fig. 13. Effect of the creep parameter c on (a) the increment of differential settlements during the 50-year creep and (b) the ratio of final differential settlement to that at $t = T_0$.

quantified using the ratio of the final differential settlement observed at $t = T_0 + 50$ year, $(s_8 - s_7)_f$ or $(s_7 - s_1)_f$, to the corresponding immediate differential settlement at $t = T_0$, $(s_8 - s_7)_0$ or $(s_7 - s_1)_0$. Fig. 13(b) indicates that the differential settlement ratios vary with c similarly to $\Delta(s_7\text{-}s_1)$ and $\Delta(s_8\text{-}s_7)$, with peak ratios occurring at c values between 0.005 and 0.01, which are typical of several siliceous sands [36]. Although c values significantly affect the absolute magnitude of differential settlements, as observed in Figs. 12(c) and 12(d), the relative magnitude of post-construction differential settlements is only moderately sensitive to c.

4.3. Effect of construction duration T_0

Fig. 14 presents the variation of the load distribution factors and differential settlements with time for the simulations where T_0 was varied from 1 week to 5 years while other parameters were kept constant. At $t = T_0$, greater values of Q_{max}/Q_{min} and CoV are observed in the simulations with lower T_0. This is because a faster loading application involves less creep settlement of footings during the loading stage. However, the figure also shows that the load distribution factors and differential settlements at the end of the simulations are almost the same irrespective of T_0. Therefore, T_0 actually controls the relative magnitudes of immediate and post-construction differential settlements but has little influence on the absolute magnitude of differential settlements in the long term.

The conclusion is consistent with Fig. 15 which shows that both the post-construction differential settlement and the differential settlement ratios decrease with the increase of T_0. Fig. 15 suggests that the post-construction load redistribution is more significant in structures with lower T_0, implying that for quickly constructed structures, it is important to consider the time-dependent behaviour of footings as the loads on lightly loaded footings may increase considerably due to the post-construction load redistribution.

4.4. Effect of mobilised strength ratio (R_{mob})

Fig. 16 presents the variation of the load distribution factors and differential settlements with time for the simulations where R_{mob} was varied from 0.05 to 0.4 while other parameters were kept unchanged. The highest R_{mob}= 0.4 corresponds to a global safety factor of the structure of 2.5 and the safety factor of centre footings should be even smaller. This means that the considered range of R_{mob} is wide enough to reflect the strength mobilisation state of most real-life structures.

Figs. 16(a) and 16(b) suggest that the distribution of footing loads is more uniform at higher levels of strength mobilisation. This is because functional footing stiffness decreases as the mobilised bearing capacity ratio increases, and load distribution becomes more uniform as relative structure–soil stiffness decreases, as implied in Fig. 4(b). The effect of R_{mob} is more significant than that of the number of loading stages (NS) and the construction duration (T_0), but is of a similar order to the effect of the creep parameter (c).

Fig. 17(a) shows the effect of the mobilised strength ratio on the increase of differential settlements between $t = T_0$ and $t = T_0 + 50$ years. With the increase of R_{mob}, both $\Delta(s_7\text{-}s_1)$ and $\Delta(s_8\text{-}s_7)$ increase, suggesting that the post-construction load redistribution is greater in structures at higher levels of strength mobilisation. However, in Fig. 17(b), it is observed that the relative magnitude of post-construction differential settlements generally decreases as R_{mob} increases. This suggests that immediate differential settlement increases faster with R_{mob} than post-construction differential settlement. This phenomenon occurs because the foundation settlements simulated by the macro-element model include a purely plastic part and a time-dependent part. Most purely plastic settlements occur during load application, adding to the sensitivity of immediate settlement to R_{mob}. Besides, although structures with low R_{mob} values are expected to have large differential settlement ratios, long-term differential settlement and load redistribution should not be a concern for such structures as overall differential settlements are small, as demonstrated in Figs. 16(c) and 16(d).

Based on Figs. 13(b), 15(b), and 17(b), it is concluded that a 5% to

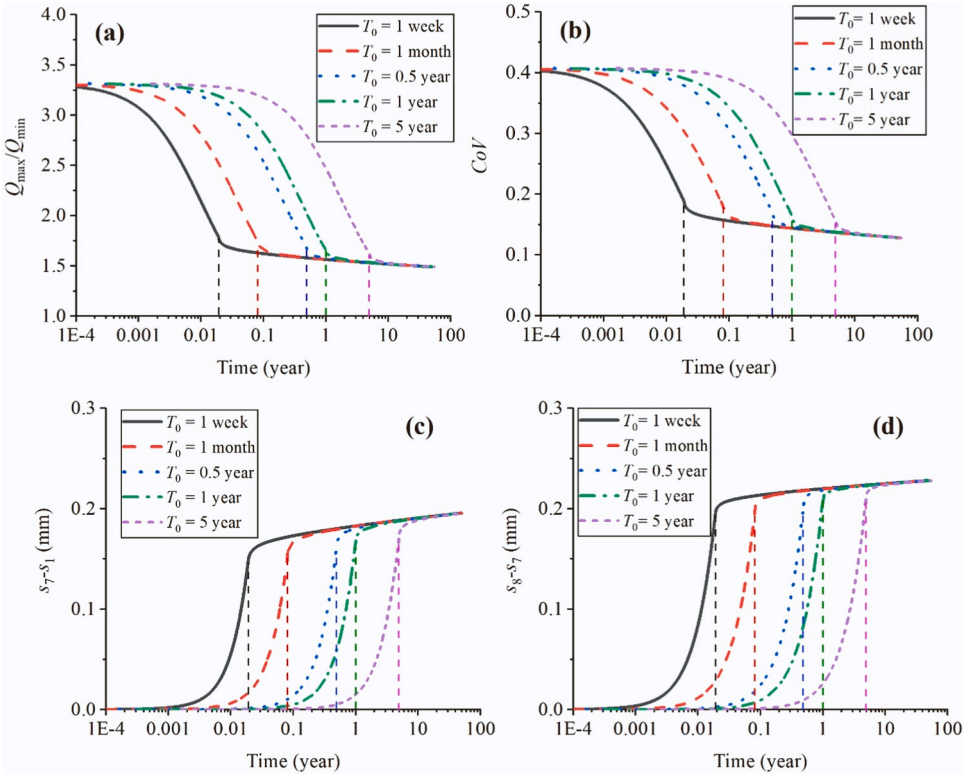

Fig. 14. Effect of T_0 on the load distribution factors and differential settlements: (a) Q_{max}/Q_{min}, (b) CoV, (c) s_7-s_1 and (d) s_8-s_7.

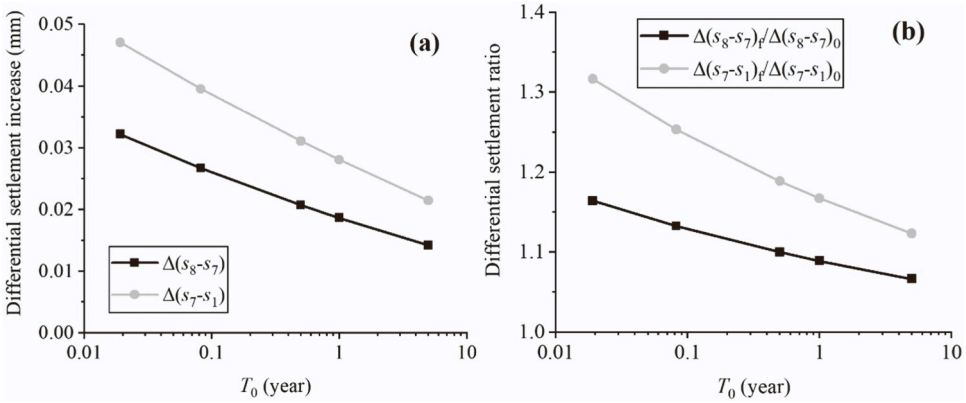

Fig. 15. Effect of T_0 on (a) the increment of differential settlements during the 50-year creep and (b) the ratio of final differential settlement to that at $t = T_0$.

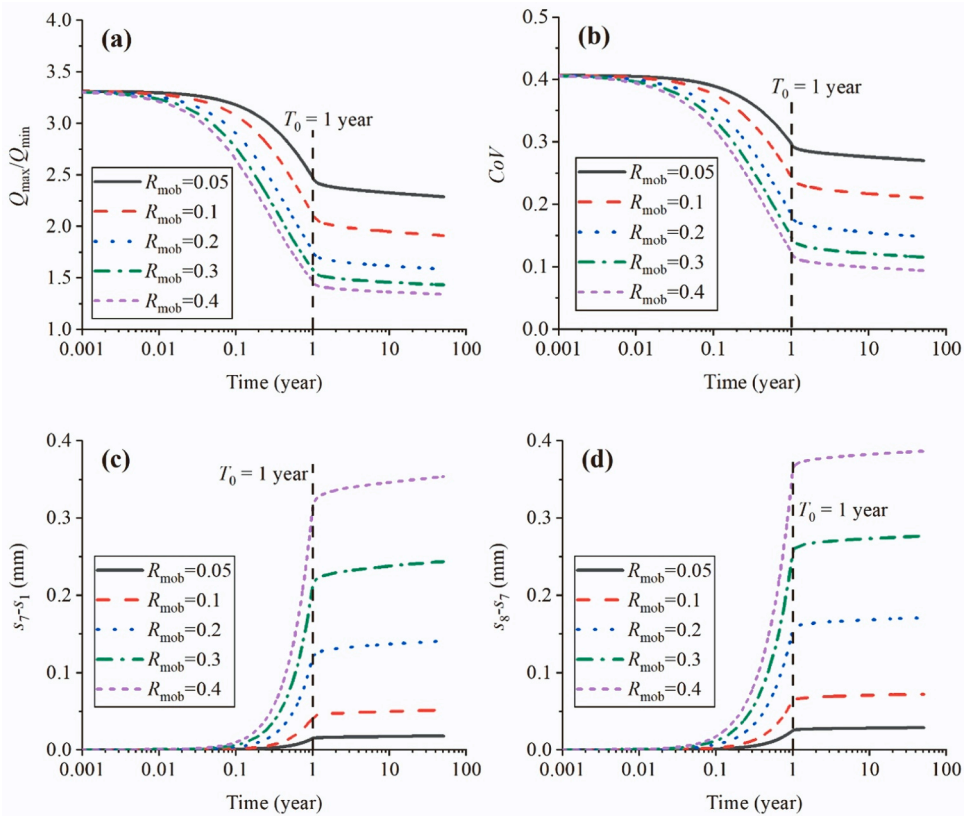

Fig. 16. Effect of mobilised strength ratio (R_{mob}) on the load distribution factors and differential settlements: (a) Q_{max}/Q_{min}, (b) CoV, (c) s_7-s_1 and (d) s_8-s_7.

35% increase of differential settlement can be expected during the 50-year creep stage for a structure on sand subjected to relatively stable working loads. Furthermore, post-construction load redistribution due to foundation creep can be significant for structures that are quickly constructed/loaded (Fig. 15(b)) or at high levels of strength mobilisation (Fig. 17(a)). However, it is worth noting that factors such as the presence of dynamic loads [57,58], non-uniformly distributed loads, variation of groundwater level [59] and soil variability [3] may increase differential settlement, leading to additional long-term load redistribution. The influence of these factors on time-dependent SSI should be studied further.

5. Conclusions

A numerical method was developed to integrate a 1D elasto-viscoplastic macro-element footing model with the structural analysis to simulate the time-dependent soil–structure interaction (SSI) in framed structures on sand. The effectiveness of the proposed method was validated through numerical models and centrifuge tests performed by the authors, demonstrating its applicability to routine SSI analysis. Parametric analyses were performed to study the factors affecting the time-dependent SSI, which leads to the following conclusions:

(1) The extent of creep-induced load redistribution in a structure increases significantly with the increase of the strength mobilisation levels of the foundations. The creep behaviour of footings on sand facilitates the load redistribution from footings with higher strength mobilisation levels to those with lower strength mobilisation levels.
(2) The rate of load application on a structure does not affect the load distribution between footings in the long term. However, a slower

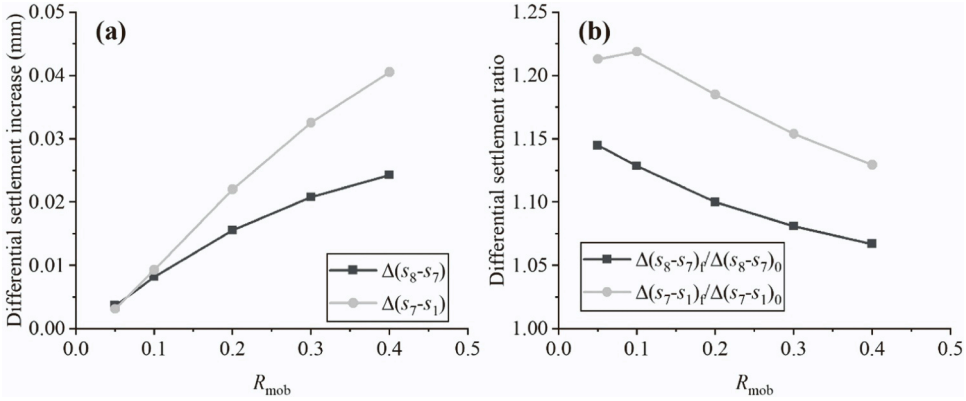

Fig. 17. Effect of mobilised strength ratio (R_{mob}) on (a) the increment of differential settlements during the 50-year creep and (b) the ratio of final differential settlement to that at $t = T_0$.

loading application results in more creep-induced load redistribution during loading and consequently less load redistribution after loading.

(3) The long-term SSI should be considered for structures that are quickly constructed or at high levels of strength mobilisation (low factor of safety).

(4) In general, the differential settlement of a structure on sand under relatively constant working loads is expected to increase by 5% to 35% after 50 years of creep.

CRediT authorship contribution statement

Jianfeng Xue: Writing – review & editing, Supervision, Methodology, Investigation, Funding acquisition, Formal analysis. **Bo LIU:** Writing – original draft, Validation, Software, Methodology, Formal analysis, Data curation, Conceptualization. **Zhenyu Yin:** Writing – review & editing. **Barry M. Lehane:** Supervision, Methodology.

Declaration of Competing Interest

The authors declare that they have no known competing financial interests or personal relationships that could have appeared to influence the work reported in this paper.

Data availability

Data will be made available on request.

Acknowledgement

The project is funded by the Special Research Grants program, The University of New South Wales (UNSW), Canberra. The first author received TFS and HDR Completion scholarships from UNSW for his PhD research.

References

[1] DeJong J, Morgenstern NR. The influence of structural rigidity on the foundation loads of the CN tower, Edmonton. Can Geotech J 1971;8:527–37.
[2] Liu B, Xue J, Lehane BM. Centrifuge investigation of soil–foundation–superstructure interaction under static loading. Eng Struct 2023; 281:115779. https://doi.org/10.1016/j.engstruct.2023.115779.
[3] Houy L, Breysse D, Denis A. Influence of soil heterogeneity on load redistribution and settlement of a hyperstatic three-support frame. Géotechnique 2005;55: 163–70. https://doi.org/10.1680/geot.2005.55.2.163.
[4] Brown P.T. The significance of structure-foundation interaction. 2nd Aust. - New Zeal. Conf. Geomech., Brisbane, Australia: 1975, p. 79–82.
[5] Poulos H.G. Settlement analysis of structural foundation systems. 4th Southeast Asian Conf. soil Eng., Kuala Lumpur, Malaysia: 1975, p. 54–62.
[6] Allam MM, Rao SKS, Subramanya BVV. Frame soil interaction and winkler model. Proc Inst Civ Eng 1991;91:477–94.
[7] Chakrabarti SC, Nayak GC, Agarwala SK. Effect of sequence of construction in the analysis of multistoreyed building frame. Build Environ 1978;13:1–6. https://doi.org/10.1016/0360-1323(78)90002-1.
[8] Brown PT, Yu SKR. Load sequence and structure-foundation interaction. J Struct Eng 1986;112:481–8. https://doi.org/10.1061/(ASCE)0733-9445(1986)112:3(481).
[9] Goschy B. Soil-foundation-structure-interaction. J Struct Div 1978;104:749–61.
[10] Farouk H, Farouk M. Effect of floor rigidity on contact stress and differential settlement. Recent Adv Mater Anal Monit Eval Found Bridg Eng 2014:94–101.
[11] Viladkar MN, Godbole PN, Noorzaei J. Space frame-raft-soil interaction including effect of slab stiffness. Comput Struct 1992;43:93–106. https://doi.org/10.1016/0045-7949(92)90083-C.
[12] Leung YF, Klar A, Soga K, Hoult NA. Superstructure–foundation interaction in multi-objective pile group optimization considering settlement response. Can Geotech J 2017;54:1408–20. https://doi.org/10.1139/cgj-2016-0498.
[13] Hora MS. Nonlinear interaction analysis of infilled frame-foundation beam-homogeneous soil system. Couple Syst Mech 2014;3:267–89.
[14] Arapakou AE, Papadopoulos VP. Factors affecting differential settlements of framed structures. Geotech Geol Eng 2012;30:1323–33. https://doi.org/10.1007/s10706-012-9546-x.
[15] Ko J, Cho J, Jeong S. Nonlinear 3D interactive analysis of superstructure and piled raft foundation. Eng Struct 2017;143:204–18. https://doi.org/10.1016/j.engstruct.2017.04.026.
[16] Leung YF, Klar A, Soga K. Theoretical study on pile length optimization of pile groups and piled rafts. J Geotech Geoenviron Eng 2010;136:319–30. https://doi.org/10.1061/(asce)gt.1943-5606.0000206.
[17] Lehane BM, Jardine RJ. Effects of long-term pre-loading on the performance of a footing on clay. Géotechnique 2003;53:689–95. https://doi.org/10.1680/geot.53.8.689.37397.
[18] Jardine RJ, Lehane BM, Smith PR, Gildea PA. Vertical loading experiments on rigid pad foundations at Bothkennar. Geotechnique 1995;45:573–97. https://doi.org/10.1680/geot.1995.45.4.573.
[19] Briaud J-L, Nicks J, Rhee K, Stieben G. San Jacinto Monument case history. J Geotech Geoenviron Eng 2007;133:1337–51. https://doi.org/10.1061/(ASCE)1090-0241(2007)133.
[20] Burland JB, Burbidge MC. Settlement of foundations on sand and gravel. Proc Inst Civ Eng 1985;vol. 78:1325–81. https://doi.org/10.1680/iicep.1986.537.
[21] Canepa Y., Depresles D. Catalogue des essays de chargement de foundations superficielles realises sur sites par les L.P.C. (1978–1990), DOSSIER 8622. Vaux-Le-Pénil, France: 1990.
[22] Peng Y, Liu H, Li C, Ding X, Deng X, Wang C. The detailed particle breakage around the pile in coral sand. Acta Geotech 2021;16:1971–81. https://doi.org/10.1007/s11440-020-01089-2.
[23] Kuwajima K, Hyodo M, Hyde AF. Pile bearing capacity factors and soil crushabiity. J Geotech Geoenviron Eng 2009;135:901–13. https://doi.org/10.1061/(asce)gt.1943-5606.0000057.
[24] Poulos HG, Chua EW, Hull TS. Settlement of model footings on calcareous sand. Geotech Eng 1984;15:21–35.
[25] Chamecki S. Structural rigidity in calculating settlements. J Soil Mech Found Div 1956;82(1):9.
[26] King GJW, Chandrasekaran VS. An assessment of the effects of interaction between a structure and its foundation. Proc. Br. Geotech. Soc. Conf. Settl. Struct. Cambridge, UK: Pentech Press; 1974. p. 368–83.
[27] King GJW, Chandrasekaran VS. Interactive analysis of a rafted multistorey space frame resting on an inhomogeneous clay stratum. Proc. Int. Conf. Finite Elem. Method Eng. University of New South Wales; 1974. p. 493–509.
[28] Viladkar MN, Ranjan G, Sharma RP. Soil-structure interaction in the time domain. Comput Struct 1993;46:429–42. https://doi.org/10.1002/9780470697771.
[29] Ai ZY, Chu ZH, Cheng YC. Time-dependent interaction between superstructure, raft and layered cross-anisotropic viscoelastic saturated soils. Appl Math Model 2021; 89:333–47. https://doi.org/10.1016/j.apm.2020.07.018.

[30] Nasri V, Magnan JP. Effect of soil consolidation on space frame-raft-soil interaction. J Struct Eng 1997;123:1528–34. https://doi.org/10.1061/(ASCE)0733-9445(1997)123.
[31] Hight DW, Leroueil S. Characterisation of soils for engineering purposes. In: Tan TS, Phoon KK, Hight DW, Leroueil S, editors. Characterisation Eng. Prop. Nat. soils. Lisse, the Netherlands: Swets and Sitlinger; 2003. p. 255–362.
[32] Jardine RJ, Standing JR, Kovacevic N. Lessons learned from full scale observations and the practical application of advanced testing and modelling. Deform Charact Geomaterials Recent Investig Prospect 2005:201–45.
[33] Shen S, Wu H, Cui Y, Yin Z. Long-term settlement behaviour of metro tunnels in the soft deposits of Shanghai. Tunn Sp Technol 2014;40:309–23.
[34] Liu B, Lehane BM, Xue J. A one–dimensional elasto-viscoplastic macro-element model for creep analysis of shallow foundations on sand. Comput Geotech 2022;142:104561. https://doi.org/10.1016/j.compgeo.2021.104561.
[35] Nova R, Montrasio L. Settlements of shallow foundations on sand. Géotechnique 1991;41:243–56.
[36] Liu B. Creep behaviour of shallow foundations on sand and its implication to soil–structure interaction. University of New South Wales, 2023.
[37] Zhang C, Tao M-X. Strong-column–weak-beam criterion for reinforced concrete frames subjected to biaxial seismic excitation. Eng Struct 2021;241:112481. https://doi.org/10.1016/j.engstruct.2021.112481.
[38] Hain SJ, Lee IK. Rational analysis of raft foundation. J Geotech Eng Div 1974;100:843–60.
[39] Fang S. The use of substructural analysis method for superstructure-foundation interaction. J Build Struct 1980;1:71–9.
[40] Naghdi PM, Murch SA. On the mechanical behavior of viscoelastic/plastic solids. J Appl Mech 1963;30:321–8. https://doi.org/10.1115/1.3636556.
[41] Olszak W., Perzyna P. The consttutive equations of the flow theory for a nonstationary yield condition. Proc., 11th Int. Congr. Appl. Mech., Berlin: Springer; 1966, p. 545–543.
[42] Timoshenko SP, Goodier JN. Theory of elasticity. McGraw-Hill; 1970.
[43] Tatsuoka F, Sato T, Park C, Kim Y, Mukabi J, Kohata Y. Measurements of elastic properties of geomaterials in laboratory compression tests. Geotech Test J 1994;17:80–94. https://doi.org/10.1520/GTJ10076J.
[44] Lehane B, Cosgrove E. Applying triaxial compression stiffness data to settlement prediction of shallow foundations on cohesionless soil. Proc Inst Civ Eng Geotech Eng 2000;143:191–200. https://doi.org/10.1680/geng.2000.143.4.191.
[45] Gazetas G, Tassoulas JL, Dobry R, O'Rourke MJ. Elastic settlement of arbitrarily shaped foundations embedded in half-space. Geotechnique 1985;35:339.
[46] Brothers PW, Sinclair GB, Segedin CM. Uniform indentation of the elastic half-space by a rigid rectangular punch. Int J Solids Struct 1977;13:1059–72. https://doi.org/10.1016/0020-7683(77)90076-2.
[47] Baraldi D, Tullini N. Static stiffness of rigid foundation resting on elastic half-space using a Galerkin boundary element method. Eng Struct 2020;225:111061. https://doi.org/10.1016/j.engstruct.2020.111061.
[48] Lehane BM, Doherty JP, Schneider JA. Settlement prediction for footings on sand. 4th Int Symp Deform Charact Geomaterials 2008:133–50.
[49] Mayne P.W., Dasenbrock D. Direct CPT method for 130 footings on sands. In: Zhang X., Cosentino P.J., Hussein M.H., editors. Innov. Geotech. Eng. Honor. Jean-Louis Briaud, Orlando, Florida: 2018, p. 135–146.
[50] Liu Q, Lehane BM. A centrifuge investigation of the relationship between the vertical response of footings on sand and CPT end resistance. Géotechnique 2021;71:455–65. https://doi.org/10.1680/jgeot.19.P.253.
[51] Su L, Lu J, Elgamal A, Arulmoli AK. Seismic performance of a pile-supported wharf: three-dimensional finite element simulation. Soil Dyn Earthq Eng 2017;95:167–79. https://doi.org/10.1016/j.soildyn.2017.01.009.
[52] Coleman JL, Bolisetti C, Whittaker AS. Time-domain soil-structure interaction analysis of nuclear facilities. Nucl Eng Des 2016;298:264–70. https://doi.org/10.1016/j.nucengdes.2015.08.015.
[53] Forcellini D, Kalfas KN. Inter-story seismic isolation for high-rise buildings. Eng Struct 2023;275:115175. https://doi.org/10.1016/j.engstruct.2022.115175.
[54] Forcellini D. Assessment of geotechnical seismic isolation (GSI) as a mitigation technique for seismic hazard events. Geosciences 2020;10. https://doi.org/10.3390/geosciences10060222.
[55] Bagbag AA, Lehane BM, Doherty JP. Predictions of footing and pressuremeter response in sand using a hardening soil model. Proc Inst Civ Eng - Geotech Eng 2017;170:479–92. https://doi.org/10.1680/jgeen.17.00040.
[56] Schmertmann JH. The mechanical aging of soils. J Geotech Eng 1991;117:1288–330. https://doi.org/10.1061/(ASCE)0733-9410(1991)117:9(1288).
[57] Ziangirov RS, Kurmes VE. Predicting the settlement of structures under long-time, oft-repeated loadings. Soil Mech Found Eng 1981;18:112–6.
[58] Bjerrum L. Secondary settlements of structures subjected to large variations in live load. In: Kravtchenko J, Sirieys PM, editors. Rheol. Soil Mech. Berlin, Heidelberg: Springer; 1966. p. 460–71. https://doi.org/10.1007/978-3-662-39449-6_37.
[59] Cao DF, Shukla SK, Yang LQ, Guo CC, Wu JH, Wang FM. Responses of calcareous sand foundations to variations of groundwater table and applied loads. J Rock Mech Geotech Eng 2022. https://doi.org/10.1016/j.jrmge.2021.08.003.